METRICA
METRology Institutional CAtalog

ISTITUTO NAZIONALE DI RICERCA METROLOGICA
Repository Istituzionale

Anomaly Detection in Magnetic Resonance-based Electrical Properties Tomography of in silico Brains

(Article begins on next page)

27 April 2024

Anomaly Detection in Magnetic Resonance-based Electrical Properties Tomography of in silico Brains

Ožbej Golob
University of Ljubljana
Faculty of Computer and
Information Science
Ljubljana, Slovenia
ozbej.golob@gmail.com

Alessandro Arduino
Istituto Nazionale di Ricerca
Metrologica
Torino, Italy
a.arduino@inrim.it

Oriano Bottauscio
Istituto Nazionale di Ricerca
Metrologica
Torino, Italy
o.bottauscio@inrim.it

Luca Zilberti
Istituto Nazionale di Ricerca
Metrologica
Torino, Italy
l.zilberti@inrim.it

Aleksander Sadikov
University of Ljubljana
Faculty of Computer and
Information Science
Ljubljana, Slovenia
aleksander.sadikov@fri.uni-lj.si

ABSTRACT

Magnetic resonance-based electrical properties tomography (EPT) is one of the novel *quantitative* magnetic resonance imaging techniques being tested for use in clinical practice. This paper presents preliminary research and results of automated detection of anomalies from EPT images. We used in silico data based on anatomical human brains in this experiments and developed two algorithms for anomaly detection. The first algorithm employs a standard approach with edge detection and segmentation while the second algorithm exploits the quantitative nature of EPT and works directly with the measured electrical properties (electrical conductivity and permittivity). The two algorithms were compared on – as of yet – noiseless data. The algorithm using the standard approach was able to quite reliably detect anomalies roughly the size of a cube with a 14 mm edge while the EPT-based algorithm was able to detect anomalies roughly the size of a cube with a 12 mm long edge.

KEYWORDS

electrical properties tomography (EPT), magnetic resonance imaging (MRI), automatic anomaly detection, artificial intelligence

1 INTRODUCTION

The frequency-dependent electrical properties (EPs), including electrical conductivity and permittivity, of biological tissues provide important diagnostic information, e.g. for tumour characterisation [9]. EPs can potentially be used as biomarkers of the healthiness of various tissues. Previous studies, not based on magnetic resonance imaging (MRI), have shown that various diseases cause changes of EPs in the tissue [3].

Electrical properties tomography (EPT) is used for quantitative reconstruction of EPs distribution at radiofrequency (RF) with spatial resolution of a few millimetres. EPT requires no electrode mounting and, during MRI scanning, no external energy is introduced into the body other than the B_1 fields. Applied B_1

fields can easily penetrate into most biological tissues, making EPT suitable for imaging of the whole body. The MRI scans for EPT are performed using a standard MRI scanner, and its spacial resolution is determined by MRI images and quality of used B_1-mapping technique [9].

The objective of this research was to develop and evaluate algorithms to automatically detect anomalies of different sizes in the EPT images. The data consisted of in silico simulated brain scans of phantoms that either contained an anomaly or not. The evaluation was aimed towards answering whether an anomaly can be detected or not, and how large an anomaly can be (reasonably) reliably detected. This represents an initial step towards the potential clinical use of EPT.

2 METHODS

2.1 Data acquisition

The MRI acquisition of the EPT inputs has been simulated in a noiseless case. Thus, the result of the electromagnetic simulation at RF has been directly converted in the acquired data, with no further post-processing. Precisely, the B_1 field generated by a current-driven 16-leg birdcage body-coil (radius 35 cm, height 45 cm) operated both in transmission and in reception with a polarisation switch has been computed in presence of anatomical human heads with a homemade FEM–BEM code [2]. The simulations have been conducted at 64 MHz (i.e. the Larmor frequency of a 1.5 T scanner).

The acquisitions of 19 human head models from the XCAT library [6] have been simulated. The considered population is statistically representative of different genders and ages. For each head model, 10 different variants are considered:

(1) Two physiological variants with the original distribution of the biological tissues. In one case, the nominal electrical conductivity provided by the IT'IS Foundation database [5] is assigned to each tissue. In the other case, the electrical conductivity of white and grey matter is sampled from a uniform distribution that admits a variation up to 10 % with respect to the nominal value. This will be referred to as the *physiological variability* of the electrical conductivity.

(2) Eight pathological variants, in which a spherical pathological inclusion is inserted in the white matter tissue. The radius of the inclusion ranges from 5 mm to 45 mm and its

electrical conductivity is set equal to that of the white matter increased by a factor uniformly sampled from 10 % to 50 % of the nominal value, because previous experimental results have shown that pathological tissues have higher EP values than healthy tissue [7, 8]. The location of the inclusion within the head is selected with a random procedure and only its intersection with the white matter tissue is kept in the final model (see Fig. 1 panels a and d). All the pathological variants take into account the physiological variability in the determination of the white and grey matter electrical conductivity.

2.2 Reconstruction techniques

In order to retrieve the distribution of the electrical conductivity, the phase-based implementations of Helmholtz-EPT (H-EPT) and convection-reaction–EPT (CR-EPT) provided by the open-source library EPTlib [1] have been used. For each head model, the distribution of the *transceive* phase [3] (input of phase-based EPT) is obtained by linearly combining the phases of the rotating components of B_1 simulated both in transmission and in reception [1].

Since noiseless inputs are considered, the smallest filter has been used both in H-EPT and in CR-EPT. Moreover, CR-EPT has been applied for a volume tomography, with an electrical conductivity of $0.1\,\mathrm{S\,m^{-1}}$ forced at the boundaries and an artificial diffusion coefficient equal to 10^{-4} rad.

Currently, the proposed anomaly detection algorithms have been tested only on the H-EPT results.

2.3 Anomaly detection

We developed two anomaly detection algorithms: (i) a more classical approach for anomaly detection in MR images and (ii) an EPT-based approach working with direct quantitative properties estimated by the MRI-based EPT.

2.3.1 Classical approach. The classical approach uses standard techniques used for anomaly detection in MR images. This approach could be applied (also) on standard MR images as it is independent of the MRI technique. The algorithm uses noiseless EPT images, produced with Helmholtz reconstruction technique, as input data.

The algorithm receives previously segmented (this segmentation was not of interest in this research) white matter from the EPT image and detects the edges in it. The edges are detected using a simple gradient edge detection technique. The gradient is calculated for each voxel based on the directional change of electrical conductivity of neighbouring voxels. The edges are represented as borders between white matter and other brain tissues as well as borders between white matter and anomalies. Edge voxels are ignored in order to avoid H-EPT reconstruction errors, which occur at borders between tissues [4].

The algorithm then calculates median electrical conductivity of all regions as separated by the detected edges. Figure 1 shows median electrical conductivity distribution by regions in a sample image.

The k-means algorithm is then employed for the classification of regions into healthy and anomaly-containing ones. The algorithm classifies an MR image based on median electrical conductivity of each region. The anomaly location is associated with the regions detected as containing the anomaly.
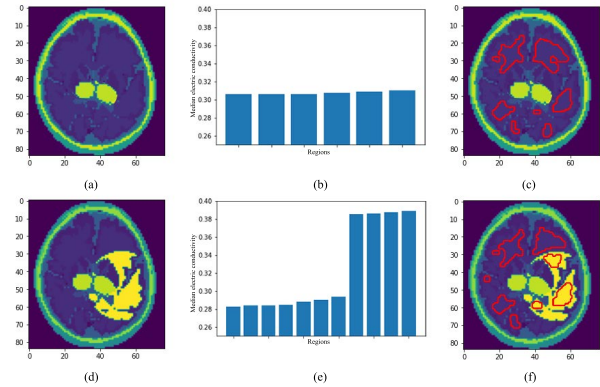

Figure 1: Median electrical conductivity distribution by regions. (a) Segmented healthy MRI image. (b) Median electrical conductivity distribution. (c) Detected regions (bordered red). (d) Segmented pathological MRI image (anomaly is yellow). (e) Median electrical conductivity distribution. (f) Detected regions (bordered red). Please note that not all of the regions are visible as only a 2D slice is shown while the data is 3D.

2.3.2 EPT approach. EPT differs from standard MRI techniques by representing EPs as quantitative values. EPs are a reliable biomarker of healthy brain. Mandija et al. [4] presented mean electrical conductivity and standard deviation of white and grey matter as a reliable measure of whether the brain contains pathological tissue.

In input data for our experiments, electrical conductivity is distributed from 90% to 110% of nominal value for white matter, and from 110% to 150% for anomalies. However, it must be noted that these are the values used for setting up the phantoms, and that these values are then only approximated when EPT reconstruction is performed. These reconstructed properties have been used as input for anomaly detection. The algorithm detects anomalies based on the difference between white matter and anomalies. The algorithm uses noiseless EPT images, produced with H-EPT, as input data.

The algorithm, as the classical one, receives as input previously segmented white matter from the whole EPT image. It then detects all voxels that have electrical conductivity between 110% and 150% of median electrical conductivity of white matter and marks them as a potential anomaly. These voxels, marked as potentially being an anomaly, are then grouped into regions based by their location. The algorithm ignores all smaller regions (below a set size threshold) that likely represent noise and reconstruction errors. All the remaining regions are classified as the anomaly.

3 RESULTS

Figure 2 shows the predictions of whether an image contains an anomaly or not for both algorithms – classical on the left (a) and EPT approach on the right (b). Each EPT image corresponds to one bar on the chart and they are arranged with the increasing size of the anomaly; the size of the bar represents the size of the anomaly in voxels. The bars are cut off at 2,000 voxels for easier viewing. Only images actually containing the anomaly are shown; for the others the false positives (FP) rate describes the performance of the two algorithms. The green colour represents correct predictions and the red colour the incorrect ones. The

Table 1: Classification evaluation of the classical approach.

Measure	Training data	Test data
Precision	0.975	1.000
Recall	0.750	0.708
F1 score	0.848	0.829
Accuracy	0.785	0.767

Table 2: Localisation evaluation of the classical approach.

Measure	Training data	Test data
IoU	0.197 ± 0.116	0.244 ± 0.110
Precision	0.932 ± 0.202	0.988 ± 0.050
Recall	0.204 ± 0.123	0.245 ± 0.110
F1 score	0.313 ± 0.163	0.379 ± 0.143

Table 3: Classification evaluation of the EPT approach.

Measure	Training data	Test data
Precision	0.976	0.971
Recall	0.769	0.708
F1 score	0.860	0.819
Accuracy	0.800	0.750

Table 4: Localisation evaluation of the EPT approach.

Measure	Training data	Test data
IoU	0.381 ± 0.140	0.435 ± 0.125
Precision	0.874 ± 0.208	0.900 ± 0.177
Recall	0.396 ± 0.142	0.450 ± 0.126
F1 score	0.535 ± 0.166	0.594 ± 0.142

yellow colour means that the algorithm correctly predicted the presence of the anomaly, but for the wrong reasons (hence Intersection over Union (IoU) is zero) – these cannot be counted as correct performance. Some misclassifications are labeled with the most likely cause: either that the anomaly is scattered in several smaller regions (each below the detection threshold size) or, in case of the EPT approach, that the anomaly is too close to the top border and is "overshadowed" by the cranium. For the unlabelled misclassifications the most likely reason is the small size of the anomaly.

Figure 2 captures rather well the minimal anomaly size where each algorithm starts performing quite reliably. The classical approach detects anomalies larger than 350 voxels and the EPT approach detects anomalies larger than 170 voxels. Since each voxel represents a cube with a 2 mm edge, these volumes translate roughly to a cube with the edge of 14 mm for the classical approach and a cube with the edge of slightly less than 12 mm for the EPT approach.

Tables 1-4 further clarify the results. The images were split into a training set, used to optimise several internal parameters and a test set for independent evaluation. Internal parameters of the classical approach specify: (i) minimum gradient value for a voxel to be recognized as an edge; (ii) electrical conductivity difference between anomaly and healthy tissue; (iii) minimum region size. Internal parameters of the EPT approach specify: (i) how many initial slices of white matter are ignored (to avoid reconstruction errors); (ii) minimum region size. The split, while random in nature, was made based on individual phantom heads – the same head with different anomalies simulated could not be both in the test and training set. The training set consisted of 130 images (including 26 not containing an anomaly), and the test set consisted of 60 images (including 12 not containing an anomaly).

Table 1 shows the results of classification evaluation of the classical approach and Table 2 shows the results of localisation evaluation using the classical approach. The localisation results are reported as mean ± standard deviation of electrical conductivity. The values for the IoU and F1 score values are lower as the result of ignoring anomaly edge voxels.

Analogously, Table 3 shows the results of classification evaluation of the EPT approach and Table 4 shows the results of localisation evaluation of the EPT approach. Again, IoU and F1

score values are reduced as the result of ignoring anomaly edge voxels.

An example of anomaly localisation is shown in Figure 3. As shown in the image, the EPT approach is generally better at anomaly localisation than the classical approach.

4 DISCUSSION AND CONCLUSIONS

The results indicate potential for future use of the EPT technique for the anomaly detection in clinical practice. The results in terms of the anomaly size are on par with what a trained radiologist is able to detect manually.

EPT, being a quantitative technique, offers the advantage of comparability of the images (e.g. in longitudinal monitoring of the patient) compared to the standard qualitative MRI. Furthermore, the direct EPT approach performed better than the classical one via edge detection. It is also less complex and this can often be a bonus in practical applications.

However, this is a pilot study and further research is required to put these approaches into actual practice. The biggest limitation of the presented study and results is that the images, while being an actual EPT reconstruction, were deliberately noiseless. With the introduction of noise the data would very much resemble the actual in vivo cases, however the obtained results will likely be worse. A lot of further work, mostly on noise reduction and detection in presence of noise is likely still required.

Moreover, currently only the data captured using H-EPT is used. This technique causes (large) reconstruction errors which occur at the borders between tissues. The results could potentially be improved by combining H-EPT and CR-EPT [1], as the latter technique does not cause reconstruction errors at borders between tissues.

The anomaly localisation could also be improved by not ignoring edges. The edges would still be removed when anomalies are detected, however, once an anomaly is detected, the edges around the anomaly could be classified as anomaly, thus improving the IoU and the F1 score.

In addition to the mean value of electrical conductivity, the standard deviation of the electrical conductivity could also be taken into account when detecting edges and anomalies.

Finally, once results achieved on EPT images of phantom brain are satisfactory, implemented approaches could be tested on in vivo data.
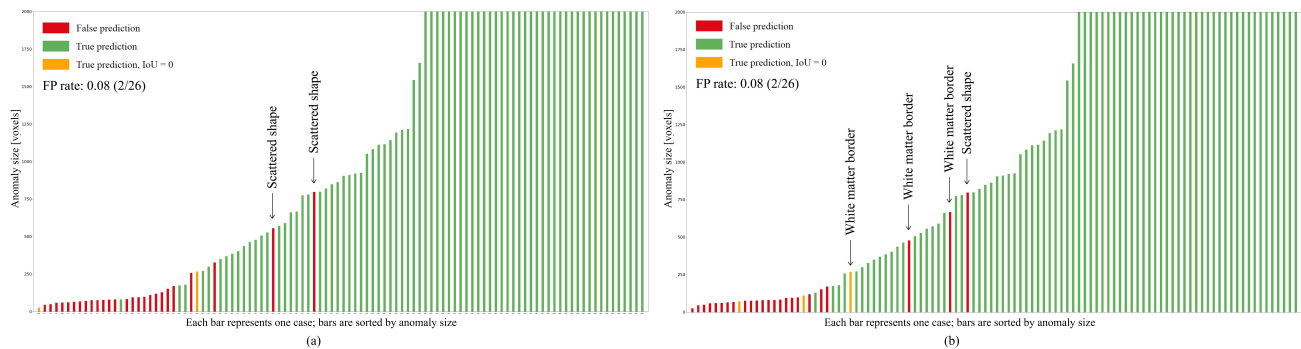
Figure 2: Predictions of anomaly detection algorithms. (a) Classical approach. (b) EPT approach.
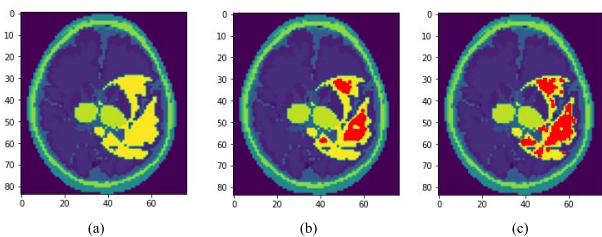

Figure 3: Anomaly localization. (a) Segmented pathological MRI image. (b) Localization of classical approach (detected anomaly is red). (c) Localization of EPT approach (detected anomaly is red).

ACKNOWLEDGMENTS

REFERENCES

[1] A. Arduino. 2021. EPTlib: an open-source extensible collection of electric properties tomography techniques. *Applied Science*, 11, 7, 3237.

[2] O. Bottauscio, M. Chiampi, and L. Zilberti. 2014. Massively parallelized boundary element simulation of voxel-based human models exposed to MRI fields. *IEEE Transactions on Magnetics*, 50, 2, 7025504.

[3] Jiaen Liu, Yicun Wang, Ulrich Katscher, and Bin He. 2017. Electrical properties tomography based on B_1 maps in MRI: principles, applications, and challenges. *IEEE Transactions on Biomedical Engineering*, 64, 11, 2515–2530. DOI: 10.1109/TBME.2017.2725140.

[4] Stefano Mandija, Petar I. Petrov, Jord J. T. Vink, Sebastian F. W. Neggers, and Cornelis A. T. van den Berg. 2021. Brain tissue conductivity measurements with MR-electrical properties tomography: an in vivo study. *Brain topography*, 34, 1, 56–63.

[5] Hasgall P.A., Di Gennaro F., C. Baumgartner, E. Neufeld, B. Lloyd, M.C. Gosselin, D. Payne, A. Klingenböck, and N. Kuster. 2018. IT'IS database for thermal and electromagnetic parameters of biological tissues. Version 4.0. (2018). DOI: 10.13099/VIP21000-04-0.

[6] W.P. Segars, B.M.W. Tsui, J. Cai, F.-F. Yin, G.S.K. Fung, and E. Samei. 2018. Application of the 4-D XCAT phantoms in biomedical imaging and beyond. *IEEE Transactions on Medical Imaging*, 37, 3, 680–692.

[7] Andrzej J. Surowiec, Stanislaw S. Stuchly, J. Robin Barr, and Arvind Swarup. 1988. Dielectric properties of breast carcinoma and the surrounding tissues. *IEEE Transactions on Biomedical Engineering*, 35, 4, 257–263.

[8] B.A. Wilkinson, Rod Smallwood, A. Keshtar, J. A. Lee, and F.C. Hamdy. 2002. Electrical impedance spectroscopy and the diagnosis of bladder pathology: a pilot study. *The Journal of urology*, 168, 4, 1563–1567.

[9] Xiaotong Zhang, Jiaen Liu, and Bin He. 2014. Magnetic-resonance-based electrical properties tomography: a review. *IEEE Reviews in Biomedical Engineering*, 7, 87–96. DOI: 10.1109/RBME.2013.2297206.